METALS AND MATERIALS International, Vol. 13, No. 2 (2007), pp. 103~107

Electron Back Scattering Diffraction (EBSD) Analysis of Hypereutectic Al-Si Alloys Modified by Sr and Sc

Myunghan Kim*

Department of Advanced Materials Engineering, Chungbuk National University,
12, Gaesin-dong, Cheongju-si, Chungbuk 361-763, Korea

In hypereutectic Al-Si alloys, Sr exists on the surfaces of primary Si phases as well as eutectic Si phases and can change the growth mode of the primary Si from non-faceted to faceted as the amount of Sr increases beyond 0.04 wt.%. However, Sc exists in the α-Al matrix instead of on the surface of the Si phases and does not significantly affect the growth mode of the primary Si phases. EBSD analysis suggests that until over-modification occurs a fraction of the twin boundary increases as the amounts of Sc and Sr increase. The twin boundary is a high-angle special boundary that occurs at a 60 degree misorientation angle.

Keywords: EBSD, growth mode, twin boundary, misorientation angle

1. INTRODUCTION

The Si phase in Al-Si alloys is a traditional nonmetallic element that grows in a faceted way as a form of polygonal primary Si or as an irregular plate form of eutectic Si. However, a small amount of impure atoms such as Na or Sr can change the growth mode of the Si phase and modify the faceted eutectic Si into non-faceted fine fibrous eutectic Si. This phenomenon has been used to improve the cast and mechanical properties of Al-Si alloys. A series of studies was carried out to clarify the mechanism that enables a change in the growth mode to affect the size and shape of eutectic Si [1,2]. However, this research was not successful until the early 1980s when transmission electron microscopy (TEM) was used to examine the inner microstructure of eutectic Si. The use of TEM has enabled researchers to study how Na and Sr affect the growth mode of eutectic Si [3,4]. The results of that research have established, firstly, that the growth of plate eutectic Si is due to the twin plane re-entrant edge (TPRE) mechanism, where the Si phase grows parallel to the existing Si twin plane; and, secondly, that the growth of the fibrous eutectic Si is due to the occurrence of abundant twinning inside the eutectic Si [4]. This phenomenon occurs when a modifier element such as Na or Sr is added.

Electron back scattering diffraction (EBSD) analysis is another efficient way of analyzing the growth orientation of crystals. EBSD patterns, which are obtained by the same principle as Kikuchi patterns [5], enable the grain orientations in polycrystals to be measured in terms of the misorientation angles between the grains. Kikuchi patterns are obtained when the incident electron beam to the specimen loses a tiny amount of energy through inelastic collisions and then reflects again.

Through the use of the EBSD technique, the grain boundary characteristics and the growth mode of an alloy can be analyzed [6-9].

EBSD analysis was adopted to study the modification effects of adding Sr and Sc to hyper-eutectic Al-Si alloys. In this approach, examinations are made of the grain boundary characteristics of Si crystals where the growth mode changes during modification.

2. EXPERIMENTAL METHOD

The first step was to prepare Al-20 wt.%Si-0.04(0.08, 01.6) wt.%Sr and Al-20 wt.%Si-0.2(0.4, 0.8, 1.6) wt.%Sc alloy melts in a high-frequency 50 KW induction furnace, by using Al-20 wt.%Si, Al-2 wt.%Sc, and Al-1 wt.%Sr alloys as mother alloys. The melts were degassed with high purity Ar for 10 min through a graphite tube immersed in the melts. Next, the melts were poured into a preheated cast iron mold (100 mm × 50 mm × 50 mm) at 800 °C. The alloy samples were collected from the center of the ingot and polished with abrasive paper (CW220-4000) and a polishing cloth (0.05 um alumina power); they were then etched with an etching agent (2 ml HF and 100 ml water). The drying of the samples was followed by ultrasonic cleaning in alcohol for 20 min.

Line scanning and mapping analysis were then conducted

*Corresponding author: myunghan@chungbuk.ac.kr

with an electron probe micro analyzer (EPMA, CAMECA-SXR) to examine the distribution of Sr and Sc in the samples. In addition, a field emission gun scanning electron microscope (Hitachi, model S-4300SE) was used to obtain the EBSD patterns of the samples, which, in turn, were used to examine the grain boundary characteristics and the growth mode of the prepared alloys. Finally, the grain orientations in the samples were analyzed with the aid of the EBSD patterns, and the boundaries of the coincidence site lattice were identified by measuring the misorientation angles between the grains [6-9].

3. RESULTS AND DISCUSSION

3.1. The microstructures of primary Si in Al-Si-Sr and Al-Si-Sc alloys

Figure 1 shows how the microstructure of hypereutectic Al-20 wt.%Si alloys change in relation to the amount of Sr present. In the Sr-free microstructure of Fig. 1(a), the typically coarse faceted primary Si crystals can be observed. However, when 0.04 wt.% of Sr is added to the alloy as in Fig. 1(b), a portion of non-faceted skeletal primary Si, as well as faceted primary Si, can be observed [10]. Finally, all the primary Si changes to non-faceted crystals when the amount of Sr is increased to 0.08 wt.%, as in Fig. 1(c), and 0.16 wt.%, as in Fig. 1(d). Figure 2 shows the results of the EPMA analysis for when 0.08 wt.% Sr, as in Fig. 2(a), and 0.16 wt.%Sr, as in Fig. 2(b), was added to the Al-20 wt.%Si alloy, respectively. The existence of Sr absorbed on the surface of primary Si has been identified elsewhere [11]. The small amount of Sr absorbed on primary Si can prevent the TPRE growth mode and induce an impurity-induced twinning (IIT) growth mode [4]. The microstructural change of the primary Si in Fig. 1 results from the change in this growth mechanism of the primary Si, which is caused by the addition of a small amount of Sr to the Al-20 wt.%Si alloys.

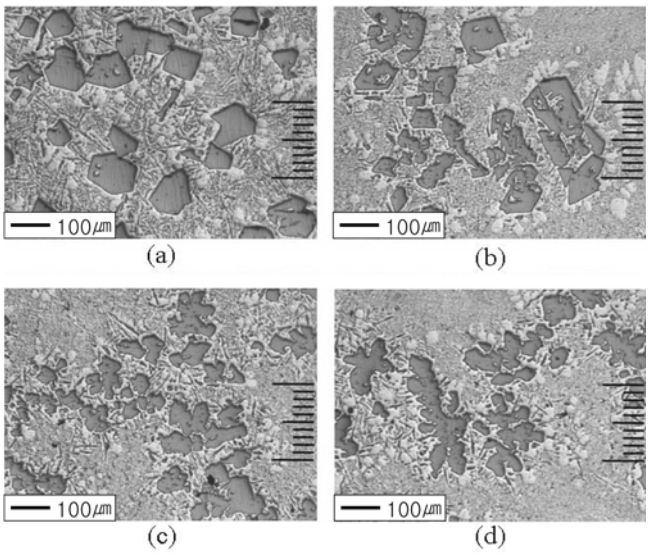

Fig. 1. Primary Si morphologies in Al-20 wt.%Si alloys according to the addition of Sr: (X50). (a) unmodified, (b) 0.04 wt.% Sr, (c) 0.08 wt.% Sr; and (d) 0.16 wt.% Sr.

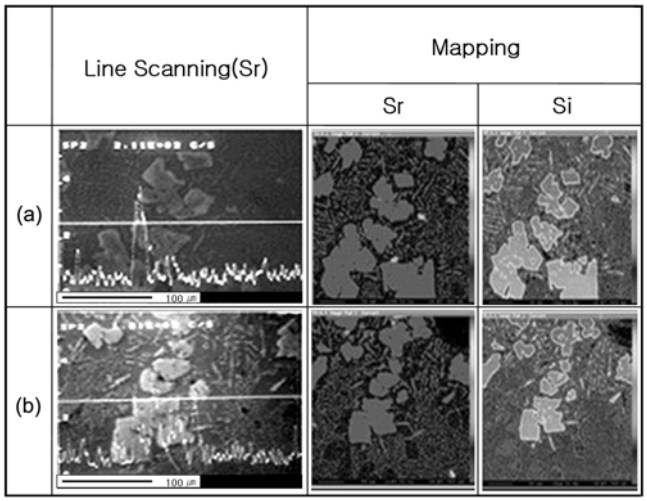

Fig. 2. EPMA analysis of the primary Si phase in Al-20 wt.%Si alloy modified by (a) 0.08 wt.%Sr and (b) 0.16 wt.%Sr.

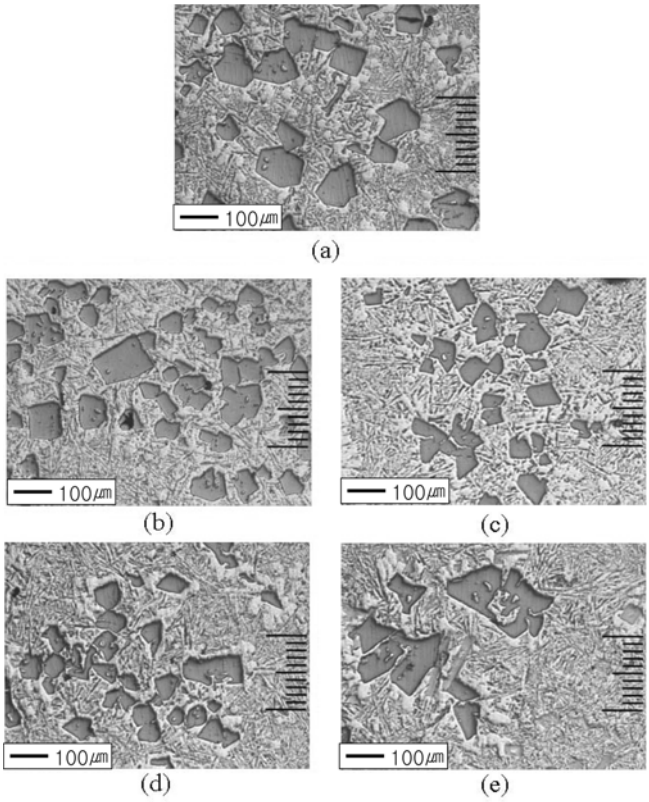

Fig. 3. Primary Si morphologies in Al-20 wt.%Si alloys according to the addition of Sc: (X50). (a) unmodified, (b) 0.2 wt.%Sc, (c) 0.4 wt.%Sc, (d) 0.8 wt.%Sc, and (e) 1.6 wt.%Sc.

Figure 3 shows the microstructural change of the primary

Si in relation to the addition of Sc to the Al-20 wt.% alloys. Here, very coarse faceted Si crystals can be observed in an unmodified state, as shown in Fig. 3(a), and at 0.2 wt.%Sc, as shown in Fig. 3(b). The shape and size of the primary Si at 0.2 wt.%Sc does not change at all. However, when 0.4 wt.%Sc, as shown in Fig. 3(c), and 0.8 wt.%Sc, as shown in Fig. 3(d), are added to the alloys, smaller polygonal shapes of the primary Si are observed. When 1.6 wt.%Sc is added to the alloys, the average size of the polygonal primary Si increases slightly and does not decrease. This phenomenon shows the over-modification phenomenon that results from the excessive addition of modifiers [12]. Moreover, the results of Figs. 3(a) to (e) show that the addition of Sc to the Al-20 wt.%Si alloys does not significantly affect the modification of the primary Si, as can be seen in the Sr-added Al-20 wt.%Si alloys.

Figure 4 shows the EPMA analysis used to locate the distribution of Sc in Al-20 wt.%Si-0.2 wt.%Sc and Al-20 wt.%Si-0.4 wt.%Sc alloys, respectively. Here, Sc is not shown on the primary Si or on the eutectic Si; rather, it is found only in the α-Al matrix.

Figure 5 shows a magnified microstructure of the alloy in Fig. 3 to which 1.6 wt.%Sc was added. Rectangular precipitates can be observed in the primary Si as well as in the α-Al matrix. Furthermore, the EPMA analysis in Fig. 6 shows that these precipitates are metallic Sc phases, which grow independently from the primary Si phases. This type of metallic Sc, which generally occurs upon the cooling down of Al-Si alloy melts with oversaturated Sc, causes a drastic decrease of the Sc solubility in the α-Al matrix [13]. In addition, metallic Sc precipitates also begin to occur in the 0.8 wt.%Sc-added alloy, though they are too fine to be observed; and the very coarse metallic Sc can occur only in 1.6 wt.%Sc-added alloy. The upper right section of Fig. 6 shows the EBSD map for the metallic Sc. Although the map shows that the metallic Sc looks like a faceted crystal, in fact it is not really a faceted crystal but a non-faceted crystal with an unstable S/L interface. This fact was also verified by Hyde *et al.* [14].

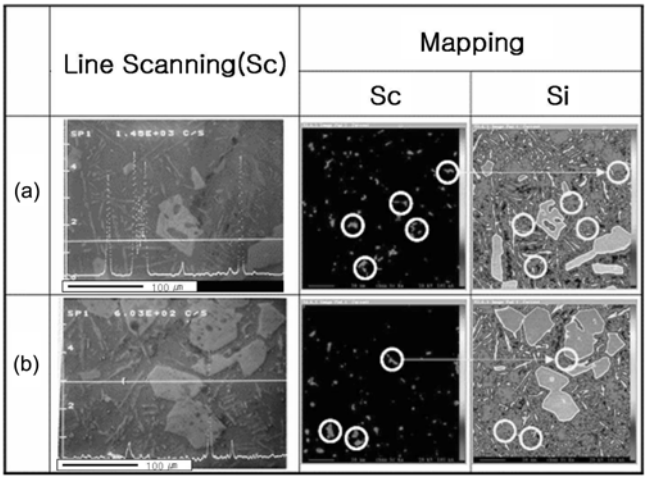

Fig. 4. EPMA analysis of the primary Si phase in Al-20 wt.%Si alloy modified by (a) 0.2 wt.%Sc and (b) 0.4 wt.%Sc.

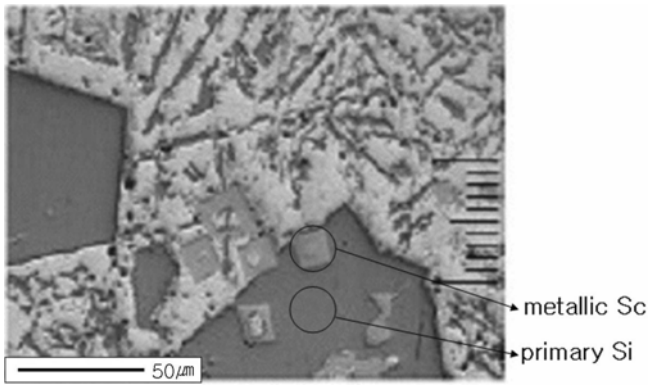

Fig. 5. The microstructure of Al-20 wt.%Si-1.6 wt.%Sc alloy, showing the rectangular precipitates within the primary Si phases as well as the α-Al matrix (X200).

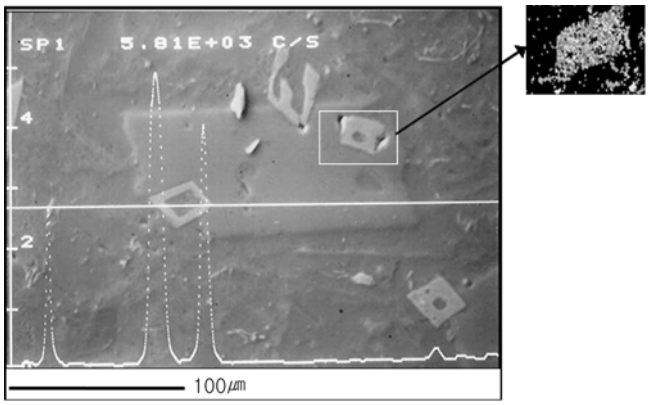

Fig. 6. The EPMA and EBSD results for the metallic Sc precipitates that appear in the Al-20 wt.%Si-1.6 wt.% Sc alloy.

3.2. EBSD analysis for Al-20 wt.%Si-Sr alloys

An EBSD analysis was performed for Al-20 wt.%Si-Sr alloys with varying Sr compositions. The results are represented in Figs. 7(a) to (d). The orientation maps in these figures represent the crystallographic orientation of each grain within the sample alloys as an inverse pole figure. The crystallographic orientation of each grain, which is represented by various colors, can be compared with the color key in Fig. 7(e) and identified. As a result, all the grain orientations within the sample alloys can be obtained and summarized.

For the EBSD analysis the step size was set to 1 um. Thus, any eutectic Si particles smaller than 1 um were excluded in the analysis, and only the eutectic Si particles that were greater than 1 um were analyzed, even though the eutectic Si particles were much larger than the primary Si particles whose colors indicated that their orientations could not be identified clearly as shown in Figs. 7(b) to (d). In these figures, the primary Si particles in each Al-20 wt.%Si-Sr alloy appear to have diverse crystallographic orientations. More-

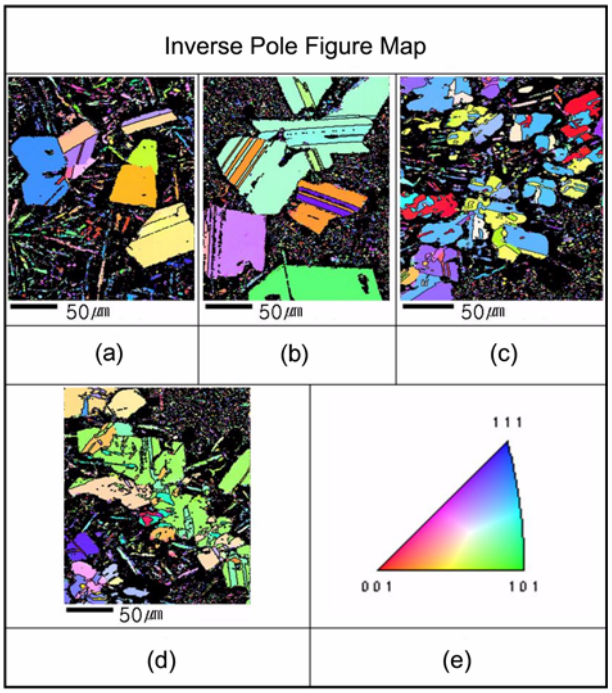

Fig. 7. An inverse pole figure map of Al-20wt.%Si alloys according to the amount of Sr, as obtained from EBSD analysis: (a) unmodified, (b) 0.04 wt.% Sr, (c) 0.08 wt.% Sr, (d) 0.16 wt.%Sr, and (e) color key.

over, the occurrence of twinning parallel to the growth direction of the primary Si crystals increases even though the polygonal primary Si shapes are nearly the same as those of unmodified Al-20 wt.%Si alloy at 0.04 wt.%Sr. However, as the amount of Sr in the alloy increases to 0.08 wt.%Sr and 0.16 wt.%Sr, the primary Si clearly changes shape from a faceted to a non-faceted form. There is a minor decrease in size, and profuse twinning occurs where many generated twin planes become entangled.

In Fig. 8, the frequency of crystallographic orientations for all the grains is represented as a histogram, which enables the crystallographic orientation of the individual grains to be analyzed and the misorientation angles between the grains to be calculated. Furthermore, the existence of a special boundary that has a specific misfit angle from a specific crystallographic axis can be identified in this histogram. The analysis indicates that one of the special Σ3 boundaries in the primary Si crystals is a twin boundary that exists at the 60 degree misfit angle [6-9]. Furthermore, as the Sr is added, the frequency of the twin boundary increases in the range of 0 to 0.08 wt.% but decreases slightly when the amount of Sr reaches 0.16 wt.%. This decrease in the frequency of the twin boundary, which results from an over-modification effect caused by the addition of an excessive amount of Sr, prevents the IIT mechanism from causing a growth of the Si crystals. The results of the EBSD analysis also confirm the results of other studies which show that Sr can change the

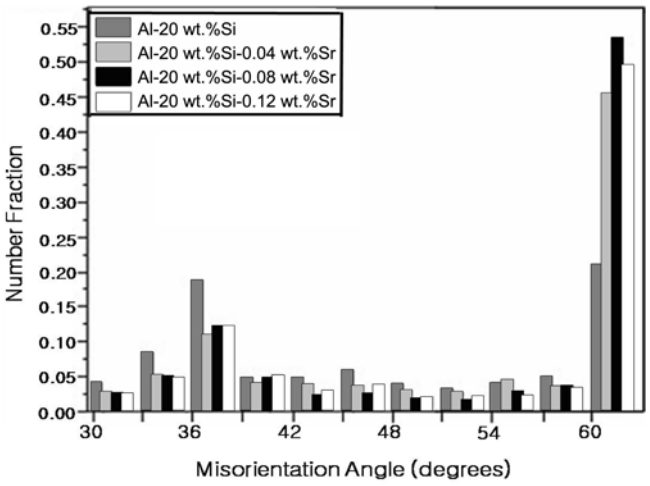

Fig. 8. The number fraction of the misorientation angle for the Si grains in the Al-20 wt.%Si alloys according to the amount of Sr.

growth mode of primary crystal from the TPRE mechanism to the IIT mechanism [3,4].

3.3. The EBSD analysis for Al-20 wt.%Si-Sc alloys

Figures 9(a) to (f) show the results of EBSD analysis for the Al-20 wt.%Si-Sc alloys with varying amounts of Sc. The results are presented as orientation maps that represent the

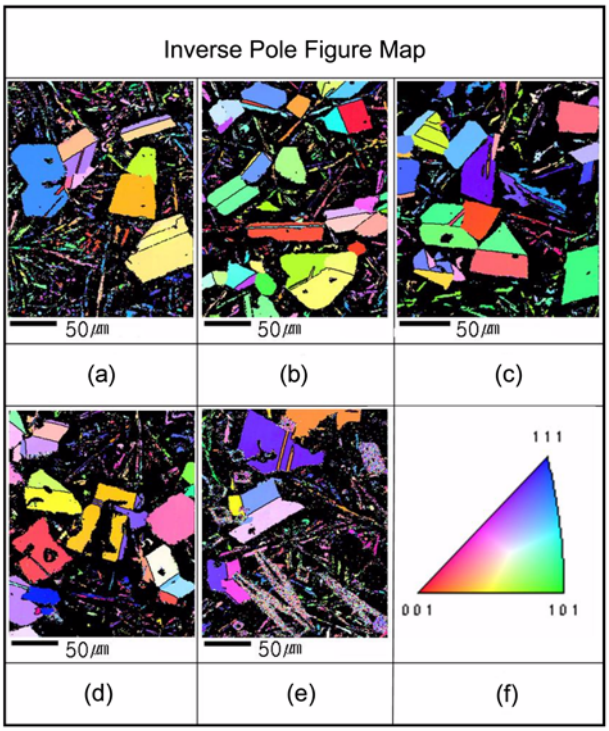

Fig. 9. An inverse pole figure map of Al-20 wt.%Si alloys according to the amount of Sc, as obtained from EBSD analysis: (a) unmodified, (b) 0.2 wt.%Sc, (c) 0.4 wt.%Sc, (d) 0.8 wt.%Sc, (e) 1.6 wt.%Sc, and (f) color key.

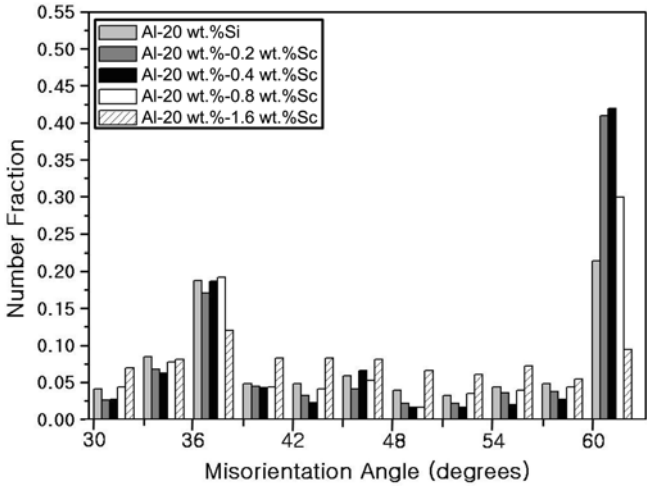

Fig. 10. The number fraction of the misorientation angle for the Si grains in the Al-20 wt.%Si alloys according to the amount of Sc.

crystallographic orientation of each grain in the sample alloys as an inverse pole figure. The primary Si crystals consist of many different crystallographic-oriented crystals, and the polygonal shapes of the primary Si crystals did not change at all as the amount of Sc increased. However, there was an increase in twinning as well as a slight decrease in the size of the primary Si.

Figure 10 shows a histogram that represents the frequency of the crystallographic orientation of all the grains in the Al-20 wt.%Si-Sc sample alloy. The histogram is based on analysis of the crystallographic orientation of the individual grains and a calculation of the misorientation angles between the grains. A special boundary with a specific misfit angle from a specific crystallographic axis can also be identified in the histogram. Based on these results, one of the special Σ3 boundaries in the primary Si crystals appears to be a twin boundary at the 60 degree misfit angle. The twin boundary corresponds to that found in the EBSD analysis for the Al-20 wt.%Si-Sr alloys.

The frequency of the twin boundary increased with the addition of Sc in the range of 0.2 to 0.4 wt.%. However, when the amount of Sc reached 1.6 wt.%, the frequency dropped drastically to less than half the value of the unmodified Al-20 wt.%Si alloy. This drastic decrease in the frequency of the twin boundary, as well as an increase in the frequency of other grain boundaries, indicates the formation of a new phase, which, as mentioned, is a metallic Sc precipitate. The results shown in the histogram indicate that there is a relatively large frequency change in the twin boundary, even though Sc does not affect the size and shape of the primary Si crystal. The relatively large frequency change in the twin boundary is caused mainly by the modification of the eutectic Si by Sc.

4. CONCLUSION

EBSD analysis, along with analysis of the crystallographic orientation of Si crystals, was used to interpret the modification effects of the addition of Sr and Sc in hypereutectic Al-Si alloys. The results of the analysis have led to the following conclusions:

1. In Al-20 wt.%Si alloys, Sc has no effect on the growth mode of the primary Si, even though Sr changes the growth mode of the primary Si from a faceted to a non-faceted mode when the amount of Sr exceeds a certain level (0.08 wt.%).

2. In Al-20 wt.%Si alloys, Sr is absorbed uniformly on the surfaces of primary Si and eutectic Si and can promote IIT growth. As a result, the frequency of the twin boundary, which is a special Σ3 boundary, increases until it reaches a peak at 0.08 wt.%Sr; it then decreases above this level as a result of the over-modification effect.

3. In Al-Si alloys, Sc is distributed only on the α-Al matrix instead of on primary and eutectic Si. There is no effect on the size and shape of the primary Si, even though there is some effect on the modification of the eutectic Si. Thus, that fact that the frequency of the twin boundary increases with the addition of Sc is due to the twinning in the eutectic Si instead of the primary Si. This increase reaches a peak value at 0.4 wt.%Sc and then drastically decreases due to the over-modification effect of the precipitating metallic Sc.

REFERENCES

1. D. C. Jenkinson and L. M. Hogan, *J. Crystal Growth* **28**, 171 (1975).
2. S. M. D. Glenister and R. Elliott, *Metal. Sci.* **15**, 181 (1981).
3. S. Z. Lu and A. Hellawell, *J.Crystal Growth* **73**, 316 (1985).
4. S. Z. Lu and A. Hellawell, *Metall. Trans. A* **18**, 1721 (1987).
5. J.-J Fundenberger, A. Morawiec, E. Bouzy, and J. S. Lecomte, Ultramicroscopy **96**, 127 (2003).
6. V. Randle, *Mater. Characterization* **47**, 411 (2001).
7. G. Palumbo, K. T. Aust, E. M. Lehockey, U. Erb, and P. Lin, *Scripta mater.* **38**, 1685 (1998).
8. M. Kumar, W.E. King, and A. J. Schwartz, *Acta mater.* **48**, 2081 (2000).
9. S. L. Wright, and R. J. Larsen, *J. Microscopy* **205**, 245 (2002).
10. A. A. Chernov, *J. Crystal Growth* **24-25**, 11 (1974).
11. M. H. Kim, Y. M. Hong, and H. Y. Cho, *Met. Mater.-Int.* **10**, 513(2004).
12. L. Baeckerud, G. Chai, and J. Tamminen, *Solidification Characteristics of Aluminum Alloys (v.2)*, p. 29, AFS/Skanaluminum, USA (1986).
13. L. S. Toropora, D. G. Eskin, M. L. Kharakterava, and T. V. Dobatkina, *Advanced Aluminum Alloys Containing Scadium*, p. 152, Gordon and Breach Science Publishers, Russia (1998).
14. K. B. Hyde, A. B. Norman, and P. B. Prangnell, *Acta mater.* **49**, 1327 (2001).